https://doi.org/10.1007/s41230-022-1122-2

Design and preparation of aluminum alloy with high thermal conductivity based on CALPHAD and first-principles calculation

Ye Wang[1], Hui-jun Kang[2, 3], *Yu Guo[1, 4], Hong-tao Chen[1], Mao-liang Hu[1], and Ze-sheng Ji[1]

1. School of Materials Science and Chemical Engineering, Harbin University of Science and Technology, Harbin 150004, China

2. Key Laboratory of Materials Modification by Laser, Ion and Electron Beams (Dalian University of Technology), Ministry of Education, Dalian 116024, Liaoning, China

3. Key Laboratory of Solidification Control and Digital Preparation Technology (Liaoning Province), School of Materials Science and Engineering, Dalian University of Technology, Dalian 116024, Liaoning, China

4. School of Science and Engineering, Huzhou College, Huzhou 313000, Zhejiang, China

Abstract: To obtain the aluminum alloy with high thermal and mechanical properties, the effects of alloying elements and the second phases on the thermal conductivity of Al alloys were investigated by CALPHAD and first-principles calculation, respectively. The properties of the second phases, including Young's modulus, Poisson's ratio and minimum thermal conductivity, were systematically studied. Results show that the ranking order of the effects of the alloying elements on the thermal conductivity is Mg>Cu>Fe>Si, and for Al-12Si alloys, the mathematical model of the relationship between the alloying elements and the thermal conductivity can be expressed as $\lambda=ax^2-bx+c$ when the second phase precipitates in the matrix. All kinds of ternary phases of Al-Fe-Si have higher deformation resistance, rigidity, theoretical hardness, Debye temperature and thermal conductivity than the other phases which possibly exist in the Al-12Si alloys. Based on the guidance of CALPHAD and first-principles calculation, the optimized chemical composition of Al alloy with high conductivity is Al-11.5Si-0.4Fe-0.2Mg (wt.%) with a thermal conductivity of 137.50 $W \cdot m^{-1} \cdot K^{-1}$ and a hardness of 81.3 HBW.

Keywords: design and preparation; CALPHAD; first-principles calculation; thermal conductivity; aluminum alloy

CLC numbers: TG146.21 **Document code:** A

1 Introduction

With the increasing requirements of light weight alloys, aluminum alloys are extensively used in automotive, aerospace and various areas due to their low densities, acceptable mechanical properties and good castability [1-4], especially in the applications such as electric vehicles, high-performance computers and LED lighting systems [5-7], which require components with both complex geometries and high heat dissipation performance. Additionally, these components also require high thermal conductivity and mechanical properties in most cases. The mechanical properties of aluminum casting alloys are commonly improved with the addition of alloying elements, but some elements such as Cr, V, Li, Mn, Ti, Zr, etc. have a serious effect on the resistivity of aluminum alloy [8-10]. Although some other elements, such as Si, Mg, Cu, and Fe, have less effect on the resistivity of aluminum alloy [11-13], the addition of these elements is certainly to reduce the thermal conductivity of aluminum alloy, because the elements solubilized in the matrix will disturb the electron and phonon transport path [14, 15]. For instance, the reduction of dissolved silicon [16, 17] or copper [18] atoms in the matrix can increase the thermal diffusivity. This means the change of resistivity caused by the alloying of different elements can be evaluated as an important reference for the thermal conductivity of aluminum alloy. Moreover, if the addition of elements exceeds the maximum solid solubility in the matrix, the formation of the second phase can also reduce the thermal conductivity [19, 20]. Thus, the effects of the multiple alloying elements on the solid solubility in the matrix and the second phase should be investigated before the design and preparation of aluminum alloy with high thermal conductivity.

In recent years, the thermal conductivity of

***Yu Guo**

Female, Ph.D. Her research interests mainly focus on preparation of aluminum alloy with high thermal conductivity.

E-mail: guoyuhrbust@163.com

Received: 2021-06-19; Accepted: 2021-11-03

binary and ternary aluminum alloys has been reported [21-25]. However, compared with the well-developed studies on mechanical properties, there is relatively scarce information on thermal conductivity of multi-component aluminum alloys due to the high economy and time cost of the experiment. Moreover, it is especially difficult to measure the compounds in aluminum alloys by experimental method [26]. Hence, it is necessary to investigate the thermal and mechanical properties of the possible intermetallics and phases in aluminum alloys. The effective thermal conductivity of multiphase systems can be estimated according to the distribution, volume fractions, structural stability, mechanical (elastic) and electronic properties of constituent phases based on CALPHADs and first-principles calculations [27-30], which will provide theoretical basis for practical application and quantitative design of aluminum alloys with high thermal conductivity.

In this study, the effects of the four common alloying elements, including Si, Mg, Cu and Fe, and their corresponding compounds on the thermal conductivity of aluminum alloys were investigated quantitatively by CALPHADs and first-principles calculations. Then, according to the analysis of the calculation results, the composition design and preparation of aluminum alloy with high thermal conductivity were implemented by the experiment. Finally, by combining with calculation results and the experimental results, the composition of the aluminum alloy with high thermal conductivity was determined and optimized.

2 Computational and experimental procedures

2.1 Calculation details

The first-principles calculations were implemented by means of the Cambridge sequential total energy package (CASTEP) [31] based on the density functional theory (DFT) [32] to investigate the mechanical properties and thermal conductivity of the various second phases in Al alloys. The exchange-correlation potential was approximated by the generalized gradient approximation (GGA) with the Perdew-Burke-Ernzerhof (PBE) function [33], and the crystal structures were optimized by Brodyden-Fletcher-Goldfarb-Shanno (BFGS) algorithm [34]. The interaction between the ions and valence electrons was described by the ultra-soft pseudo potential method. To obtain the precise results in the calculation of geometric optimization and elastic constant, the plane-wave cut-off energy (E_{cut}), k-points meshes for Brillouin zone (BZ), the self-consistent field (SCF) tolerance energy, the mean Feynman-Hellmann force (F-H) acting on each atom, the maximum stress in the unit cell (S_M), and the maximum atomic displacement (D_M) used in this work are all listed in Table 1. The crystal structures of the second phases in Al-Si alloys are shown in Figs. 1–3, respectively, and the lattice parameters of the second phases are summarized in Table 2.

Table 1: Parameters used for first-principles calculations

Phase	E_{cut} (eV)	k-point	SCF tolerance energy (eV/atom)	F-H (eV/Å)	S_M (GPa)	D_M (Å)
Al_2Cu	340	7×7×6				
Mg_2Si	340	7×7×7				
$Al_3Fe_2Si_3$	550	8×6×4				
$Al_2Fe_3Si_3$	550	13×9×9	Total energy changes $>5\times10^6$	<0.01	<0.02	$<5\times10^4$
$Al_2Fe_3Si_4$	550	15×5×5				
$Al_8FeMg_3Si_6$	340	4×4×4				
$Al_9FeMg_3Si_5$	340	4×4×4				

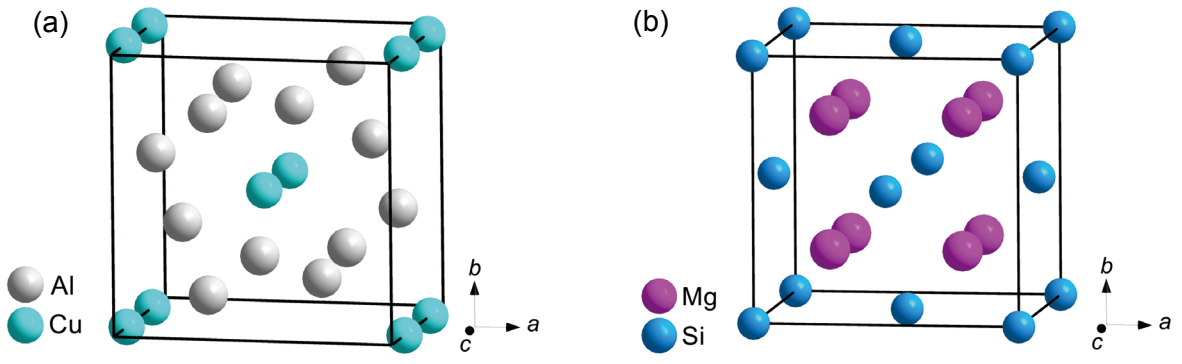

Fig. 1: Schematic diagram of cell structure of Al_2Cu (a) and Mg_2Si (b)

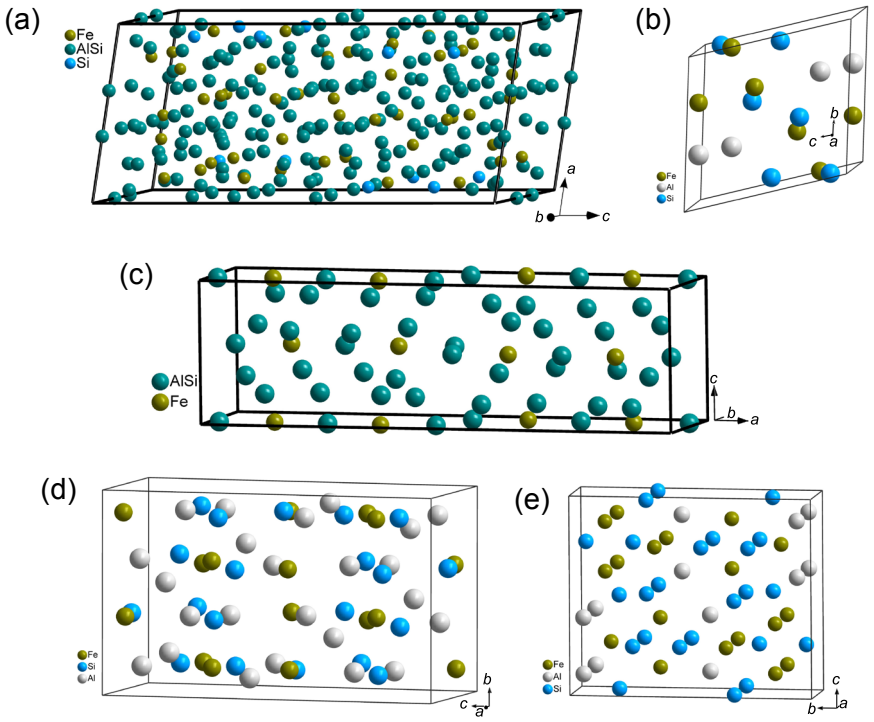

Fig. 2: Crystal structures of AlxFeySiz compounds: (a) α-Al-Fe-Si; (b) $Al_2Fe_3Si_3$; (c) β-Al-Fe-Si; (d) $Al_3Fe_2Si_3$; (e) $Al_2Fe_3Si_4$

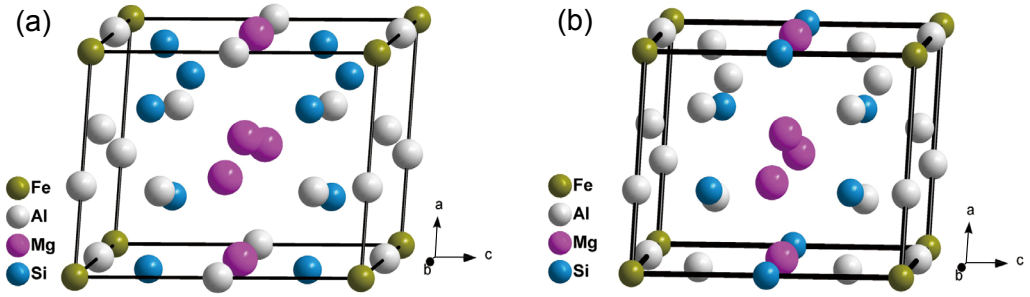

Fig. 3: Schematic diagram of cell structures of $Al_8FeMg_3Si_6$ (a) and $Al_9FeMg_3Si_5$ (b)

To characterize the properties of the second phases in Al-Si alloys, elastic constants C_{ij} were calculated by the strain-stress method based on Hooke's law [36]. And the elastic constants can be used to judge the mechanical stability according to the Born stability criterion [36]. The tetragonal crystal of Al_2Cu has six independent elastic constants (C_{11}, C_{12}, C_{13}, C_{33}, C_{44} and C_{66}), and the restrictions of the Born stability criterion are as follows [37]:

$$\begin{gathered} C_{11}-C_{12}>0 \\ C_{33}(C_{11}+C_{12})-2C_{13}^2>0 \\ C_{44}>0 \\ C_{66}>0 \end{gathered} \quad (1)$$

For the cubic crystal of Mg_2Si, the restrictions of the Born stability criterion are determined by three independent elastic constants (C_{11}, C_{12} and C_{44}) [38]:

$$\begin{gathered} C_{11}-C_{12}>0 \\ C_{11}+2C_{12}>0 \\ C_{44}>0 \end{gathered} \quad (2)$$

For the monoclinic crystal of $Al_3Fe_2Si_3$, the restrictions of the Born stability criterion are determined by thirteen independent elastic constants (C_{11}, C_{12}, C_{13}, C_{15}, C_{22}, C_{23}, C_{25}, C_{33}, C_{35}, C_{44}, C_{46}, C_{55} and C_{66}) [37]:

$$\begin{gathered} C_{ii}>0,\ i=1,2,3,4,5,6 \\ C_{33}C_{55}-C_{35}^2>0,\ C_{44}C_{66}-C_{46}^2>0,\ C_{22}C_{33}-C_{23}^2>0 \\ C_{11}+C_{22}C_{33}+2(C_{12}+C_{13}+C_{23})>0 \\ C_{22}(C_{33}C_{55}-C_{35}^2)+2C_{23}C_{25}C_{35}-C_{25}^2C_{55}-C_{25}^2C_{33}>0 \\ 2[C_{15}C_{25}(C_{33}C_{12}-C_{13}C_{23})+C_{15}C_{35}(C_{22}C_{13}-C_{12}C_{23}) \\ +C_{25}C_{35}(C_{11}C_{23}-C_{12}C_{13})]-[C_{15}^2(C_{22}C_{33}-C_{23}^2) \\ +C_{25}^2(C_{11}C_{33}-C_{13}^2)+C_{35}^2(C_{11}C_{22}-C_{12}^2)]+C_{55}>0 \end{gathered} \quad (3)$$

Table 2: Lattice parameters used for first-principles calculations

Phase	Crystal system	Space group	Lattice constant	Atom number					
				Total	Al	Si	Cu	Mg	Fe
Al_2Cu	Tetragonal	I4/mcm	*a*=*b*=0.6067 nm, *c*=0.4877 nm	12	8	-	4	-	-
Mg_2Si	Cubic (FCC)	Fm-3m	*a*=*b*=*c*=0.6351 nm	12	-	4	-	8	-
α-Al_8Fe_2Si	Hexagonal	P63/mmc	*a*=*b*=1.2404 nm, *c*=2.6234 nm	Site occupancy (SOF) ≠ 1					
$Al_3Fe_2Si_3$	Monoclinic	P21/c	*a*=0.7179 nm, *b*=0.8354 nm, *c*=1.4155 nm	64	24	24	-	-	16
β-Al_5FeSi	Monoclinic	C12/c1	*a*=2.0813 nm, *b*=0.6175 nm, *c*=0.6161 nm	Site occupancy (SOF) ≠ 1					
$Al_2Fe_3Si_3$	Triclinic	P-1	*a*=0.4651 nm, *b*=0.6326 nm, *c*=0.7499 nm	16	4	6	-	-	6
$Al_2Fe_3Si_4$	Orthorhombic	Cmcm	*a*=0.3669 nm, *b*=1.2385 nm, *c*=1.0147 nm	18	4	8	-	-	6
$Al_8FeMg_3Si_6$	Hexagonal	P-62m	*a*=*b*=0.662 nm, *c*=0.792 nm	18	8	6	-	3	1
$Al_9FeMg_3Si_5$	Hexagonal	P-62m	*a*=*b*=0.663 nm, *c*=0.786 nm	18	9	5	-	3	1

For the orthorhombic crystal of $Al_2Fe_3Si_4$, there are nine independent elastic constants for the restrictions of the Born stability criterion (C_{11}, C_{12}, C_{13}, C_{22}, C_{23}, C_{33}, C_{44}, C_{55} and C_{66}) [39]:

$$\begin{aligned} &C_{ii} > 0, i = 1, 2, 3, 4, 5, 6 \\ &C_{11} + C_{22} - 2C_{12} > 0 \\ &C_{22} + C_{33} - 2C_{23} > 0 \\ &C_{11} + C_{33} - 2C_{13} > 0 \\ &C_{11} + C_{22} + C_{33} + 2C_{12} + 2C_{13} + 2C_{23} > 0 \end{aligned} \quad (4)$$

For the triclinic crystal of $Al_2Fe_3Si_3$, there are twenty-one independent elastic constants. Because of the low symmetry of the crystals, the equations of the Born stability criterion are too complex to show [35]. Both $Al_9FeMg_3Si_5$ and $Al_8FeMg_3Si_6$ are hexagonal crystals, so the restrictions of the Born stability criterion are determined by five independent elastic constants (C_{11}, C_{12}, C_{13}, C_{33} and C_{44}) [40]:

$$\begin{aligned} &C_{11} - C_{12} > 0 \\ &C_{33}(C_{11} + C_{12}) - 2C_{13}^2 > 0 \\ &C_{44} > 0 \end{aligned} \quad (5)$$

2.2 Experimental method

The aluminum alloys with designed composition were fabricated by melting aluminum ingot (99.79%), magnesium ingot (99.9%), and Al-20Si, Al-10Fe and Al-30Cu master alloys in a resistance furnace at 1,023 ± 10 K for 30 min, and then poured to a permanent mold at 998 K.

The chemical composition of the alloys was tested by means of an M5000 Metal Analyzer CCD direct-reading spectrometer. X-ray diffraction analysis was carried out in X'Pert PRO using Cu-Kα radiation over $10^o \leq 2\theta \leq 90^o$ ranges, and the Brinell hardness at room temperature was tested using a HB-3000B Brinell hardness tester. The microstructures and phase characterizations were observed on the surfaces of the polished samples after etching with the solution of 4vol.% HF using the scanning electron microscopy (SEM, Thermo scientific Apreo) equipped with an energy dispersive X-ray spectrometer (EDS). The thermal diffusivity was measured on the disc-shaped samples with 12.7 mm in diameter and 2.3 mm in thickness by the LFA 1000 Laser Flash Apparatus at room temperature. The density of samples was measured by FA1004N electron balance based on Archimedes rule, and the specific heat was measured by a differential scanning calorimeter (DSC). Then, the thermal conductivity λ could be calculated by the following formula:

$$\lambda = \alpha \cdot \rho \cdot C_p \quad (6)$$

where, α is thermal diffusivity ($m^2 \cdot s^{-1}$), ρ is the density ($g \cdot cm^{-3}$) and C_p is the specific heat capacity ($J \cdot kg^{-1} \cdot K^{-1}$). In addition, all the test results are on average of at least seven measurements.

3 Results

3.1 Effects of different elements on thermal conductivity of aluminum alloys

Figure 4 gives the CALPHAD calculation results of the effects of Si, Mg, Cu and Fe with different contents on the thermal conductivity of aluminum alloys, and the inside figures in Figs. 4(b), (c) and (d) show the comparison of Mg, Cu and Fe contents with Ref. [9] in the ranges of the red boxes, respectively. It shows that the predicted and the measured results have the same varying tendency, and the difference of the two results is all about 20 $W \cdot m^{-1} \cdot K^{-1}$ in value numerically. It may be caused by some microstructures, including defects, grain boundaries, and phase boundaries, which could not be considered by the simulation. Compared the influence of Si and Mg with Cu and Fe, the minimum values of thermal conductivity of both Al-Si and Al-Mg alloys are found at a content of about 11wt.%, and after that the declines of thermal conductivity tend to stable gradually, while the thermal conductivity of Al-Cu and Al-Fe alloys decreases continuously with the increase of elements content. In comparison to Al-Si alloy, the decrease rate of the thermal conductivity of Al-Mg alloy with an increase of alloying element addition is obviously faster. The thermal conductivity of Al-Mg alloy falls to 136.9 $W \cdot m^{-1} \cdot K^{-1}$ when the content of Mg only reaches 5wt.%. Similarly, the experimental results of thermal conductivity shown in Figs. 4(c) and (d) also indicate that, compared with that of the Al-Fe alloy, the decrease rate of thermal conductivity of Al-Cu is faster as the alloying element content ranges from 0 to 1.5wt.%.

The solid solubility of the Mg and Cu is larger than that of Si and Fe inducing the large lattice distortion. Meanwhile, the intermetallic compounds formed from Mg and Cu, including Al_3Mg_2 and Al_2Cu, precipitate along grain boundaries and distribute continuously in a network, which has a great influence on the mean free path of electron transport in the matrix and then affects the thermal conductivity of the aluminum alloys [9, 41-44]. Moreover, the Si phase and intermetallic compounds of Al_3Fe are dispersed throughout the matrix. Therefore, compared with Mg and Cu, the element of Si and Fe has less effect on the thermal conductivity of the aluminum alloys.

The above investigation results indicate that the thermal conductivity of all binary aluminum alloys in this study decreases with the increase of the element addition amount. Moreover, the element Mg has the greatest influence on the thermal conductivity of aluminum alloys, followed by Cu and Fe, and Si affects the thermal conductivity of aluminum alloys insignificantly. Therefore, the element Si was designed as the main alloying element for the following study, and the near-eutectic composition with Si content of 12wt.% was selected to ensure the formability and mechanical properties of the aluminum alloys. Then, the contents of other alloying elements were optimized based on the Al-12Si alloy.

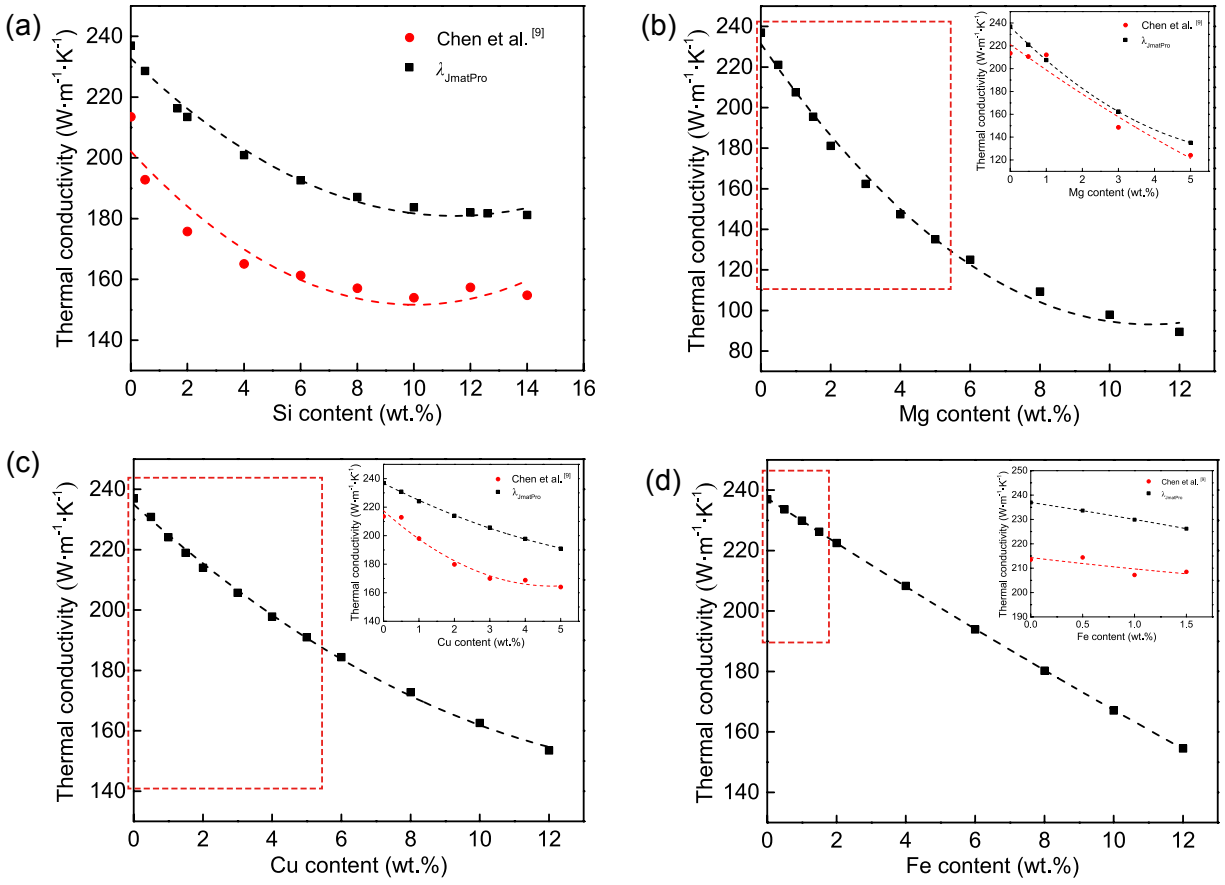

Fig. 4: Effects of contents of Si (a), Mg (b), Cu (c) and Fe (d) on thermal conductivity of aluminum alloys

3.2 Effects of different elements on thermal conductivity of Al-12Si alloy

Figure 5 illustrates the CALPHAD calculation results of the effects of Mg, Cu and Fe with different contents on the thermal conductivity of Al-12Si alloys. It can be seen that Fe has the least effect on the thermal conductivity of Al-12Si alloy when its content less than 2wt.%, and Mg has the greatest effect. In addition, the thermal conductivity of Al-12Si alloys decreases linearly when the contents of all three elements are less than 1.5wt.%. The slope of thermal conductivity curves of Al-12Si alloy decreases gradually after the contents of all three elements are more than 1.5wt.%, especially the Al-12Si-*x*Cu alloy, its thermal conductivity is even higher than that of Al-12Si-*x*Fe alloy after the content of Cu exceeds 2wt.%.

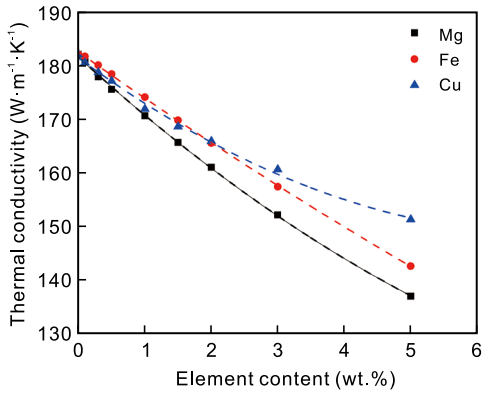

Fig. 5: Effects of Mg, Fe and Cu contents on thermal conductivity of Al-12Si alloys

3.3 Properties of second phases in Al-12Si alloys

Apparently, the addition of elements in Al-Si alloys did not only induce the formation of solid solution, but also formed many intermetallic compounds as the second phase in the matrix. Since the microstructure of alloys could be considered as the mixture of solid solution and second phase, the mechanical properties and thermal conductivity of the second phase are very important to the performances of Al-Si alloys. However, the properties of the second phase can hardly be measured experimentally. To choose the appropriate second phase, the properties of the second phase were simulated and predicted by the first-principles calculations. The calculation results of the elastic constants of the possible second phases in Al-Si alloys are listed in Table 3. According to the Born stability criterion shown as Eqs. (1) to (5), all characteristic value of the elastic constants matrix in this study are positive, which also means that the structures of all second phases are mechanically stable.

Based on the data of the elastic constants C_{ij} of the second phases, the bulk modulus B, shear modulus G, theoretical hardness H_V, Young's modulus E and Poisson's ratio v of the second phases are all calculated by the Voigt-Reuss-Hill approximation [45, 46]:

$$B = \frac{1}{2}\left(B_V + B_R\right) \tag{7}$$

$$G = \frac{1}{2}\left(G_V + G_R\right) \tag{8}$$

Table 3: Calculated elastic constants (C_{ij}, in GPa) for second phases in Al-12Si alloys

C_{ij}	Phase						
	Al_2Cu	Mg_2Si	$Al_3Fe_2Si_3$	$Al_2Fe_3Si_3$	$Al_2Fe_3Si_4$	$Al_8FeMg_3Si_6$	$Al_9FeMg_3Si_5$
C_{11}	187.5	112.7	203.6	314.0	316.4	89.5	182.9
C_{12}	69.7	22.4	87.9	75.1	92.2	78.9	52.3
C_{13}	21.1	-	117.4	66.6	71.6	37.9	39.1
C_{14}	-	-	-	−2.6	-	-	-
C_{15}	-	-	−7.6	0.1	-	-	-
C_{16}	-	-	-	10.6	-	-	-
C_{22}	-	-	228.6	322.8	278.5	-	-
C_{23}	-	-	91.4	62.7	49.5	-	-
C_{24}	-	-	-	11.3		-	-
C_{25}	-	-	10.4	2.9		-	-
C_{26}	-	-	-	4.4		-	-
C_{33}	236.5	-	185.5	320.0	20.0	139.3	165.8
C_{34}	-	-	-	−1.6	-	-	-
C_{35}	-	-	-9.6	−6.0	-	-	-
C_{36}	-	-	-	−1.0	-	-	-
C_{44}	45.1	44.3	59.1	120.2	92.2	30.7	51.0
C_{45}	-	-	-	13.8	-	-	-
C_{46}	-	-	1.3	12.8	-	-	-
C_{55}	-	-	65.3	127.8	102.0	-	-
C_{56}	-	-	-	1.9	-	-	-
C_{66}	57.0	-	52.7	129.8	110.7	-	-

$$H_V = 2\left[(G/B)^2 G\right]^{0.585} - 3 \quad (9)$$

where B_V, G_V and B_R, G_R represent the bulk modulus and shear modulus of Voigt and Reuss, respectively.

Young's modulus E and Poisson's ratio v can be obtained by the following equations subsequently [47]:

$$E = \frac{9BG}{3B+G} \quad (10)$$

$$v = \frac{3B-2G}{6B+2G} \quad (11)$$

Then, the calculation results of the mechanical properties of various secondary phases are summarized in Table 4. It can be found that the elastic modulus of Al_2Cu and all Al-Fe-Si ternary phases is generally larger than that of the others, and $Al_2Fe_3Si_3$ has the greatest deformation resistance and stiffness. According to the Pugh criteria [48], the B/G ratios of most secondary phases are smaller than 1.75, except $Al_3Fe_2Si_3$ (2.41) and $Al_8FeMg_3Si_6$ (3.98), the ternary phases, which indicates that most secondary phases are brittle, while the phases of $Al_3Fe_2Si_3$ and $Al_8FeMg_3Si_6$ are ductile. Furthermore, the results of Poisson's ratio also confirm this because a solid with v smaller than 0.26 is brittle [49]. Thus, the order of the ductility of the secondary phase is $Al_8FeMg_3Si_6$ > $Al_3Fe_2Si_3$ > Al_2Cu > $Al_9FeMg_3Si_5$ > $Al_2Fe_3Si_4$ > Mg_2Si = $Al_2Fe_3Si_3$. From the results of the theoretical hardness, it can be observed that $Al_2Fe_2Si_3$ has the highest theoretical hardness and $Al_8FeMg_3Si_6$ has the smallest theoretical hardness, which corresponds to the results of Young's modulus.

The Debye temperature is closely correlated with bond strength, structure stability and many physical properties of the material. In general, a higher Debye temperature can associate a stronger chemical bond and better thermal conductivity. Thus, in order to investigate the capability of thermal conduction of the secondary phases, the Debye temperature Θ_D and two kinds of minimum thermal conductivity λ_{min} are calculated by the following equations [50-52]:

$$\Theta_D = V_m \frac{h}{\kappa_B}\left[\frac{3n}{4\pi}\left(\frac{N_A\rho}{M}\right)\right]^{\frac{1}{3}} \quad (12)$$

$$\lambda_{min}^{Clarke} = 0.87\kappa_B\left[M/(n\cdot N_A)\right]^{-\frac{2}{3}} E^{\frac{1}{2}}\rho^{\frac{1}{6}} \quad (13)$$

$$\lambda_{min}^{Cahill\text{-}Pohl} = \frac{\kappa_B}{2.48} N^{\frac{2}{3}}\left(V_l + 2V_t\right) \quad (14)$$

where λ_{min}^{Clarke} is the minimum thermal conductivity calculated by Clarke model and $\lambda_{min}^{Cahill\text{-}Pohl}$ is the minimum thermal conductivity calculated by Cahill-Pohl model, h is the Planck's constant, κ_B is the Boltzmann's constant, N_A is the Avogadro number, ρ is the density, M is the molecular weight, n is the total number of atoms, N is the density of atoms per volume, V_m is the average sound velocity, V_t is the transverse sound velocity and V_l is the longitudinal sound velocity. Moreover, the average sound velocity, transverse sound velocity and longitudinal sound velocity can be calculated approximately by the following equations [48, 51]:

$$V = \left[\frac{1}{3}\left(\frac{1}{V_l^3} + \frac{2}{V_t^3}\right)\right]^{-\frac{1}{3}} \quad (15)$$

$$V_l = \left[\left(B + \frac{4}{3}G\right)/\rho\right]^{\frac{1}{2}} \quad (16)$$

$$V_t = \left[G/\rho\right]^{\frac{1}{2}} \quad (17)$$

where B and G are bulk modulus and shear modulus respectively, as listed in Table 4. Then, the results of the Debye temperature and minimum thermal conductivity are summarized in Table 5. The results show that the $Al_2Fe_3Si_3$ has the highest Debye temperature among them. For the quaternary phases, the Debye temperature of $Al_9FeMg_3Si_5$ is obviously higher than that

Table 4: Calculated bulk, shear and Young's modulus (GPa), Poisson's ratio v, H_V (GPa) and B/G of second phases in Al-12Si alloys

System	Elastic moduli							B/G	v	H_V
	B_V	B_R	B	G_V	G_R	G	E			
Al_2Cu	92.80	92.80	92.80	62.73	56.69	59.71	147.50	1.55	0.24	10.06
Mg_2Si	52.46	52.46	54.46	44.61	44.61	44.61	105.13	1.22	0.18	11.61
$Al_3Fe_2Si_3$	134.57	133.07	133.82	56.82	54.24	55.53	146.35	2.41	0.32	4.491
$Al_2Fe_3Si_3$	151.71	151.62	151.67	125.72	123.85	124.78	293.78	1.22	0.18	23.80
$Al_2Fe_3Si_4$	148.12	147.05	147.59	107.17	105.73	106.45	257.45	1.39	0.21	17.94
$Al_8FeMg_3Si_6$	69.75	69.69	69.72	24.23	10.79	17.51	48.47	3.98	0.38	-0.88
$Al_9FeMg_3Si_5$	88.06	87.56	87.81	60.19	59.12	59.65	145.91	1.47	0.22	10.91

of $Al_8FeMg_3Si_6$. According to the calculation results, the order of Debye temperature of the phases in the Al-Si alloy is $Al_2Fe_3Si_3$ > $Al_2Fe_3Si_4$ > $Al_9FeMg_3Si_5$ > Mg_2Si > $Al_3Fe_2Si_3$ > Al_2Cu > $Al_8FeMg_3Si_6$. Thus, generally the ternary Al-Fe-Si phases have the best thermal conductivity, which agrees well with the calculation results of the minimum thermal conductivity.

3.4 Design and preparation of Al-12Si alloy with high thermal conductivity

According to the above results of calculations, the designed Al-Si alloy does not only possess the characteristic of good thermal conductivity, but also should have excellent mechanical properties. The phases of Mg_2Si, Al_2Cu and ternary Al-Fe-Si were chosen for the design of Al-Si alloy. Because the ternary Al-Fe-Si phases always appear in the shape of a long needle, which decreases the mechanical properties of the Al-Si alloy, the content of the Fe element is relatively low (0.1wt.%). Furthermore, to avoid inducing the quaternary phases in the alloy, the formation of the second phases with different contents of Mg and Cu in Al-12Si-0.1Fe alloys was investigated by CALPHAD calculation. According to the results shown in Table 6, the ternary Al-Fe-Si phases are substituted by Mg_2Si and $Al_8FeMg_3Si_6$ when the content of the Mg element exceeds 0.3wt.%, but they are not affected by the Cu content, and the Al_2Cu phase appears in the matrix until the Cu content exceeds 2wt.%. Thus, the schemes of the designed Al-12Si alloys are listed in Table 7 based on the calculation results.

The designed Al-Si alloys in Table 7 are cast in gravity, and their measured composition, thermal conductivity and Brinell hardness are listed in Table 8, and compared with the commercial ADC12 [52] and AC3C [53] aluminum alloys. The Cu has a great impact on the thermal conductivity of the as-cast

Table 5: Debye temperature (K), sound wave velocity ($m \cdot s^{-1}$) and minimum thermal conductivity ($W \cdot m^{-1} \cdot K^{-1}$) of second phases in Al-12Si alloys

Phases	V			Θ_D	λ_{min}	
	V_t	V_l	V_m		Cahill	Clark
Al_2Cu	3,710.78	6,305.51	4,112.58	496.50	1.26	1.06
Mg_2Si	4,775.64	7,564.99	5,255.05	560.85	1.22	1.02
$Al_3Fe_2Si_3$	3,658.32	7,078.82	4,096.24	507.75	1.39	1.24
$Al_2Fe_3Si_3$	4,865.12	7,767.06	5,358.13	696.03	1.86	1.71
$Al_2Fe_3Si_4$	4,704.62	7,758.75	5,199.03	661.56	1.75	1.61
$Al_8FeMg_3Si_6$	2,490.34	5,740.09	2,812.95	327.26	0.91	0.73
$Al_9FeMg_3Si_5$	4,591.43	7,690.03	5,081.66	591.98	1.44	1.21

Table 6: Phase contents and thermal conductivity of Al-12Si-0.1Fe-(*x*Mg, *y*Cu) alloy (wt.%)

Composition	Conductivity ($W \cdot m^{-1} \cdot K^{-1}$)	Phase contents (wt.%)			
		Mg_2Si	Al_2Cu	β-AlFeSi	$Al_8FeMg_3Si_6$
Al12Si0.1Fe0.1Mg	179.37	-	-	0.76	-
Al12Si0.1Fe0.2Mg	177.89	-	-	0.6	0.39
Al12Si0.1Fe0.3Mg	176.72	0.08	-	0.35	1.02
Al12Si0.1Fe0.5Mg	174.36	0.23	-	-	1.89
Al12Si0.1Fe1Mg	169.04	1.08	-	-	1.89
Al12Si0.1Fe1.5Mg	163.93	1.79	-	-	1.89
Al12Si0.1Fe2Mg	159.34	2.64	-	-	1.89
Al12Si0.1Fe3Mg	151.3	4.06	-	-	1.89
Al12Si0.1Fe5Mg	137.54	7.35	-	-	1.9
Al12Si0.1Fe0.1Cu	178.04	-	-	-	-
Al12Si0.1Fe0.2Cu	176.53	-	-	0.75	-
Al12Si0.1Fe0.3Cu	174.76	-	-	0.75	-
Al12Si0.1Fe0.5Cu	169.85	-	-	0.75	-
Al12Si0.1Fe1Cu	163.12	-	-	0.75	-
Al12Si0.1Fe1.5Cu	157.22	-	-	0.75	-
Al12Si0.1Fe2Cu	152.16	-	0.65	0.75	-
Al12Si0.1Fe3Cu	143.52	-	2.43	0.75	-
Al12Si0.1Fe5Cu	130.65	-	6.36	0.75	-

Al-Si alloys, the content of Cu is inversely proportional to the value of thermal conductivity. The element Fe has a beneficial effect on improving the thermal conductivity of Al-Si alloys, and the effect of Mg on the thermal conductivity of Al-Si alloys is inconspicuous. Thus, the composition of the designed Al-Si alloys is optimized by adjusting the content of Fe and Mg without the addition of Cu. The optimized composition and the measured thermal conductivity and hardness of the alloys are shown in Tables 9 and 10, respectively. Obviously, the composition of No. 6 alloy has the highest thermal conductivity of 137.50 $W \cdot m^{-1} \cdot K^{-1}$ and a better hardness of 81.3 HBW. Thus, the optimal composition of the high thermal conductivity Al alloy is the 11.5wt.% Si, 0.42wt.% Fe, and 0.17wt.% Mg.

Table 7: Chemical compositions of designed Al-12Si alloys (wt.%)

Alloy No.	Si	Fe	Mg	Cu	Al
1	12	0.1	0.5	2	Bal.
2	12	0.1	0.2	2	Bal.
3	12	0.1	0.2	5	Bal.

4 Discussion

In this investigation, the principle of selecting alloying elements is that, firstly, the atomic radius between the alloying element and aluminum should be close, and thus the lattice distortion induced by alloying element solution is small. Obviously, the atomic radius of the Fe and Cu are larger than that of Al, and the

Table 8: Measured chemical compositions, thermal conductivity and hardness of designed Al-12Si alloys

Alloy No.	Element content (wt.%)								Conductivity ($W \cdot m^{-1} \cdot K^{-1}$)	Hardness (HBW)
	Si	Fe	Mg	Cu	Ni	Mn	Zn	Al		
1	11.32	0.15	0.46	2.07	0.05	0.02	0.03	Bal.	94.68	95
2	11.42	0.12	0.21	2.68	0.05	0.02	0.01	Bal.	91.02	101
3	11.42	0.11	0.17	5.25	0.04	0.02	0.01	Bal.	89.25	114
ADC12 [52]	10–12	≤0.9	≤0.30	1.5–3.5	≤0.5	≤0.5	≤1.0	Bal.	96.2	82
AC3C [53]	10–13	≤0.8	≤0.15	≤0.25	≤0.1	≤0.35	≤0.3	Bal.	121	≥50

Table 9: Optimized chemical compositions of Al-12Si alloys

Alloy No.	Element content (wt.%)			
	Si	Fe	Mg	Al
4	12	0.1	0.5	Bal.
5	12	0.1	0.3	Bal.
6	12	0.5	0.3	Bal.

Table 10: Measured chemical compositions, thermal conductivity and hardness of optimized Al-12Si alloys

Alloy No.	Element content (wt.%)								Conductivity ($W \cdot m^{-1} \cdot K^{-1}$)	Hardness (HBW)
	Si	Fe	Mg	Cu	Ni	Mn	Zn	Al		
4	11.55	0.15	0.46	-	0.05	0.02	0.09	Bal.	105.80	67.1
5	11.46	0.15	0.21	-	0.05	0.02	0.02	Bal.	97.57	62.7
6	11.49	0.42	0.17	-	0.04	0.02	0.01	Bal.	137.50	81.3
ADC12 [52]	10–12	≤0.9	≤0.30	1.5–3.5	≤0.5	≤0.5	≤1.0	Bal.	96.2	82
AC3C [53]	10–13	≤0.8	≤0.15	≤0.25	≤0.1	≤0.35	≤0.3	Bal.	121	≥50

atomic radius of the Si and Mg are close to that of Al, so Si and Mg could be selected as the main alloying element. However, the increased contents of alloying elements will theoretically reduce the thermal diffusivity of the alloy, especially when the elements dissolve in the matrix [22, 56, 57]. Therefore, secondly, the solid solubility of the alloying element in aluminum should be low. Because the solid solubility of Mg in aluminum is about 14.9wt.%, which is much higher than that of Si, the element of Si was chosen as the main alloying element at last. Finally, as another important component, the thermal properties, morphology and size of the second phase have great effects on the properties of the alloy, especially the mechanical properties and thermal properties. In order to reveal the influence of the second phase on the thermal conductivity of Al-12Si alloy preferably, the thermal conductivity of the alloys at room temperature and the contents of the second phases with different additions of Mg, Fe, Cu was calculated, as listed in Table 11. Based on the results, the relationship between the coefficient of thermal conductivity and contents of the second phases of the alloys is fitted, as shown in the following equations:

$$\lambda = 0.1876Mg^2 - 6.9854Mg + 179.6 \quad (18)$$

$$\lambda = 0.0179Fe^2 - 2.5198Fe + 182.77 \quad (19)$$

$$\lambda = 0.0799Cu^2 - 3.1425Cu + 169.77 \quad (20)$$

Among the coefficients of the equations given above, the element of Mg has the greatest damage to thermal conductivity of the alloy, due to the second phase of Mg_2Si is the typical semiconductor material and its thermal conductivity is very poor. Furthermore, because the solid solubility of the Cu element in aluminum is higher and its atomic radius is larger than those of the others, it is easy to cause relatively serious lattice distortion in the matrix, but, more than that, the Al_2Cu phase mainly distributes in a network in the matrix and has a strong scattering effect on electrons during the process of electron transmission. This can explain the low thermal conductivity of the designed alloys containing Cu. Finally, the equations also indicate that the second phase of β-AlFeSi has the least damage to the thermal conductivity of the alloy, but considering it has the greatest damage to mechanical properties of the alloy, the content of Fe should not exceed 0.5wt.% in the designed alloys, which agrees with the results of the thermal conductivity of the second phases by first-principles calculation.

Table 11: Thermal conductivity and phase contents of Al-12Si-*x*(Mg, Fe, Cu) alloys (*x*=0–5)

Composition	Conductivity ($W \cdot m^{-1} \cdot K^{-1}$)	Phase contents (wt.%)		
		Mg_2Si	β-AlFeSi	Al_2Cu
Al12Si	182.03	-	-	-
Al12Si0.1Mg	180.66	-	-	-
Al12Si0.2Mg	179.13	0.12		
Al12Si0.3Mg	177.84	0.28	-	-
Al12Si0.5Mg	175.5	0.6	-	-
Al12Si1Mg	170.57	1.25	-	-
Al12Si1.5Mg	165.61	2.22	-	
Al12Si2Mg	160.96	2.86	-	-
Al12Si3Mg	152.1	4.47	-	
Al12Si5Mg	136.93	7.7	-	-
Al12Si0.1Fe	181.68	-	0.37	-
Al12Si0.3Fe	180.04	-	1.12	-
Al12Si0.5Fe	178.36	-	1.87	-
Al12Si1Fe	174.07	-	3.37	-
Al12Si1.5Fe	169.76	-	5.62	-
Al12Si2Fe	165.51	-	7.12	-
Al12Si3Fe	157.35	-	10.88	-
Al12Si5Fe	142.55	-	18.380	-
Al12Si0.1Cu	180.51	-	-	-
Al12Si0.3Cu	178.71	-	-	-
Al12Si0.5Cu	177.11	-	-	-
Al12Si1Cu	171.87	-	-	-
Al12Si1.5Cu	168.56	-	-	0.43
Al12Si2Cu	165.85	-	-	1.22
Al12Si3Cu	160.59	-	-	3.21
Al12Si5Cu	151.27	-	-	7.2

According to the CALPHAD calculation results listed in Table 6, three second phases of Si, β-AlFeSi and $Al_8FeMg_3Si_6$ appear in the matrix of the designed alloy. In order to confirm the kind of second phase contained in the designed alloy, the x-ray diffraction (XRD) test was implemented and the results are illustrated in Fig. 6 which indicate that there are only two second phases of Si and β-AlFeSi (Al_8Fe_2Si and Al_5FeSi).

The x-ray diffraction analysis may not detect the $Al_8FeMg_3Si_6$ due to its small amount which is less than 0.39wt.% in calculation results. Thus, the energy dispersive spectroscopy (EDS) analysis was carried out coupled with scanning electron microscopy (SEM), and the analysis results of the as-cast Al-Si-Fe-Mg alloys are shown in Fig. 7. The results demonstrate that the second phase of $Al_8FeMg_3Si_6$ is substituted by the Mg_2Si. Thus, there are four second phases in the Al matrix of the designed alloy, including needlelike eutectic-Si, reticular Mg_2Si, needlelike Al_5FeSi and Al_8Fe_2Si with Chinese script shape.

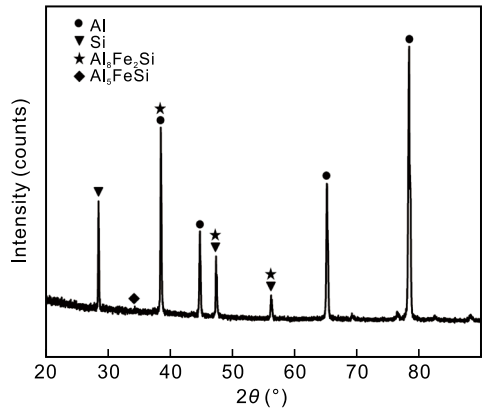

Fig. 6: XRD results of designed as-cast Al-11.5Si-0.4Fe-0.2Mg alloy

5 Conclusions

In the present study, the effects of the alloying elements on the thermal conductivity of Al alloys were investigated by CALPHAD calculation, and the properties of the second phases and their effects on the thermal conductivity of Al-Si alloys were studied by first-principles calculation. According to the results of the calculation, the chemical compositions of Al-Si alloys with high conductivity were designed and optimized, and their thermal conductivities were measured. The conclusions are drawn as follows:

(1) The thermal conductivity of aluminum alloys decreases fast with the increasing addition of the alloying elements of Si, Mg, Fe and Cu, and decreases gradually with the formation and precipitation of the second phases. The ranking order of the effects of the alloying elements is Mg>Cu>Fe>Si. Considering the manufacturability and machining properties of the aluminum alloys with high thermal conductivity, the content of the main alloying element of Si is determined as 12wt.%.

(2) Fe has less damage to the thermal conductivity of Al-12Si alloys, and on the contrary, Mg has a great influence. The mathematical model of the relationship between the alloying elements and the thermal conductivity of Al-12Si alloys can be expressed as below when the second phase precipitates in the matrix: $\lambda=ax^2-bx+c$.

(3) The calculation results of the properties of the second phases, such as Al_2Cu, Mg_2Si, and which may precipitate, ternary phases

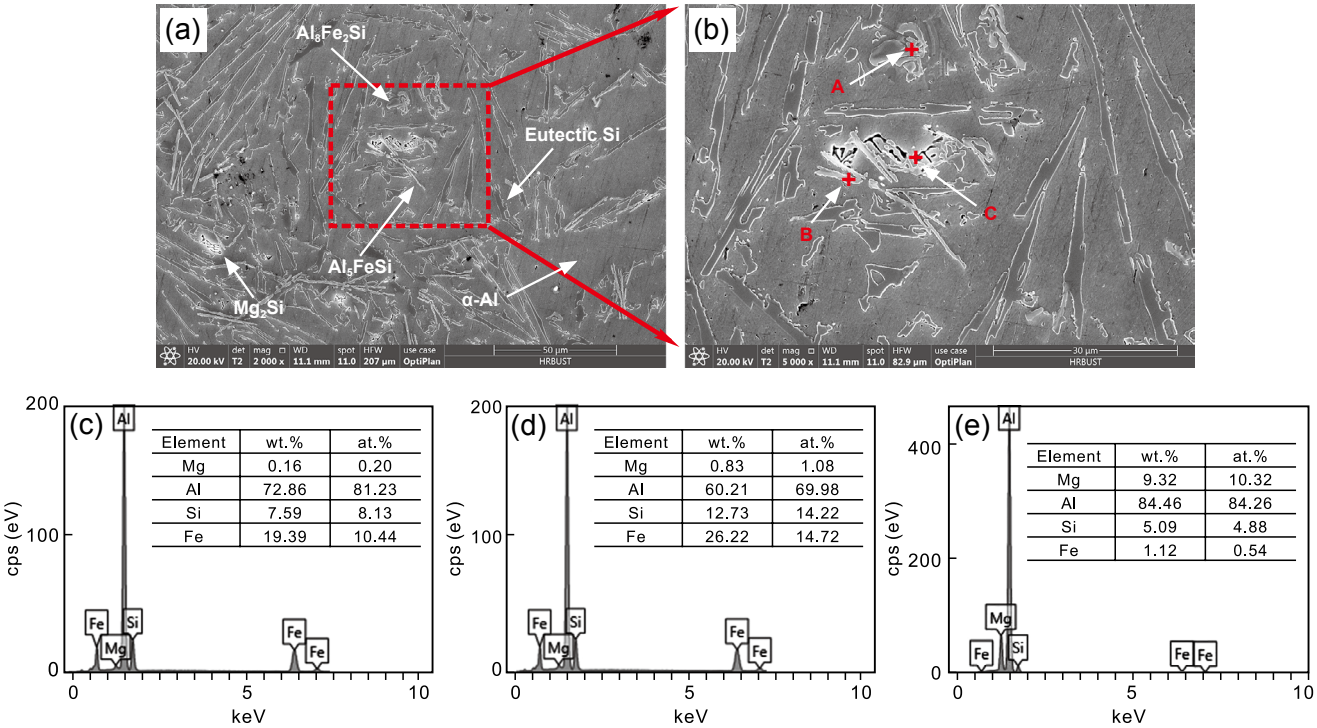

Fig. 7: SEM morphology of as-cast Al-Si-Fe-Mg alloys: (a) low-power SEM; (b) high-power SEM; (c)–(e) is EDS results of Points A–C in (b)

and quaternary phases ($Al_8FeMg_3Si_6$ and $Al_9FeMg_3Si_5$) in Al-12Si alloys indicate that the ternary phases of Al-Fe-Si (including $Al_3Fe_2Si_3$, $Al_2Fe_3Si_3$, $Al_2Fe_3Si_4$, etc.) have the best deformation resistance, rigidity and theoretical hardness. Furthermore, the Debye temperature and thermal conductivity of the ternary phases of Al-Fe-Si are also higher than those of the other phases.

(4) Based on the measurement results of the thermal conductivity and mechanical properties of the designed alloys, the optimal chemical composition of Al-Si alloy of Al-11.5Si-0.4Fe-0.2Mg (wt.%) with high thermal conductivity is obtained.

Acknowledgements

This work was financially supported by the National Natural Science Foundation of China (Nos. 51801045 and 52171113), and the Key Laboratory of Materials Modification by Laser, Ion and Electron Beams, Ministry of Education, Dalian University of Technology (No. KF2002).

References

[1] Guan R G, Shen Y F, Zhao Z Y, et al. A high-strength, ductile Al-0.35Sc-0.2Zr alloy with good electrical conductivity strengthened by coherent nanosized-precipitates. Journal of Materials Science and Technology, 2017, 33(3): 215–223.

[2] Duan S W, Matsuda K, Wang T, et al. Microstructures and mechanical properties of a cast Al-Cu-Li alloy during heat treatment procedure. Rare Metals, 2021, 40(7): 1897–1906.

[3] Lin G, Zhang Z, Wang H, et al. Enhanced strength and electrical conductivity of Al-Mg-Si alloy by thermo-mechanical treatment. Materials Science and Engineering A, 2016, 650: 210–217.

[4] Choi S W, Kim Y M, Lee K M, et al. The effects of cooling rate and heat treatment on mechanical and thermal characteristics of Al-Si-Cu-Mg foundry alloys. Journal of Alloys and Compounds, 2014, 617: 654–659.

[5] Kotiadis S, Zimmer A, Elsayed A, et al. High electrical and thermal conductivity cast Al-Fe-Mg-Si alloys with Ni additions. Metallurgical and Materials Transactions A, 2020, 51: 4195–4214.

[6] Chang J, Zhang Q, Lin Y F, et al. Layer by layer graphite film reinforced aluminum composites with an enhanced performance of thermal conduction in the thermal management applications. Journal of Alloys and Compounds, 2018, 742: 601–609.

[7] Li W P, Zhang Y L, Mao J. Enhanced strength and electrical conductivity of Al-0.3Ce alloy simultaneously with Ti(C, N) nanoparticle addition. Rare Metals, 2021, 40: 1890–1896.

[8] Liang Z, Miao J S, Shi R H, et al. CALPHAD modeling and experimental assessment of Ti-Al-Mn ternary system. CALPHAD: Computer Coupling of Phase Diagrams and Thermochemistry, 2018, 63: 126–133.

[9] Shin J S, Ko S H, Kim K T. Development and characterization of low-silicon cast aluminum alloys for thermal dissipation. Journal of Alloys and Compounds, 2015, 644: 673–686.

[10] Erol H, Çadirli E, Erol E A, et al. Dependency of the thermal and electrical conductivity on temperatures and compositions of Zn in the Al-Zn alloys. International Journal of Cast Metals Research, 2019, 32(2): 95–105.

[11] Chen J K, Hung H Y, Wang C F, et al. Thermal and electrical conductivity in Al-Si/Cu/Fe/Mg binary and ternary Al alloys. Journal of Materials Science, 2015, 50: 5630–5639.

[12] Zhang C, Du Y, Liu S H, et al. Thermal conductivity of Al-Cu-Mg-Si alloys: Experimental measurement and CALPHAD modeling. Thermochimica Acta, 2016, 635: 8–16.

[13] Kim C W, Cho J I, Choi S W, et al. The effect of alloying elements on thermal conductivity of aluminum alloys in high pressure die casting. Advance Material Research, 2013, 813: 175–178.

[14] Lumley R N, Deeva N, Larsen R, et al. The role of alloy composition and T7 heat treatment in enhancing thermal conductivity of aluminum high pressure diecastings. Metallurgical and Materials Transactions A, 2012, 44: 1074–1086.

[15] Wang Y, Lu Z X, Ruan X L. First principles calculation of lattice thermal conductivity of metals considering phonon-phonon and phonon-electron scattering. Journal of Applied Physics, 2016, 119: 225109.

[16] Choi S W, Kim Y M, Lee K M, et al. The effects of cooling rate and heat treatment on mechanical and thermal characteristics of Al-Si-Cu-Mg foundry alloys. Journal of Alloys and Compounds, 2014, 617: 654–659.

[17] Choi S W, Cho H S, Kang C S, et al. Precipitation dependence of thermal properties for Al-Si-Mg-Cu-(Ti) alloy with various heat treatment. Journal of Alloys and Compounds, 2015, 647: 1091–1097.

[18] Choi S W, Cho H S, Kumai S. Effect of the precipitation of secondary phases on the thermal diffusivity and thermal conductivity of Al-4.5Cu alloy. Journal of Alloys and Compounds, 2016, 688: 897–902.

[19] Payandeh M, Sjölander E, Jarfors A E W, et al. Influence of microstructure and heat treatment on thermal conductivity of rheocast and liquid die cast Al-6Si-2Cu-Zn alloy. International Journal of Cast Metals Research, 2015, 29(4): 202–213.

[20] Vandersluis E, Emadi P, Andilab B, et al. The role of silicon morphology in the electrical conductivity and mechanical properties of as-cast B319 aluminum alloy. Metallurgical and Materials Transactions A, 2020, 51: 1874–1886.

[21] Kim Y M, Choi S W, Hong S K. The behavior of thermal diffusivity change according to the heat treatment in Al-Si binary system. Journal of Alloys and Compounds, 2016, 687: 54–58.

[22] Stadler F, Antrekowitsch H, Fragner W, et al. The effect of main alloying elements on the physical properties of Al-Si foundry alloys. Materials Science and Engineering A, 2013, 560: 481–491.

[23] Vijayan V, Prabhu K N. The effect of Sr modification on thermal diffusivity of Al-8Si alloy. International Journal of Cast Metals Research, 2018, 31(2): 80–86.

[24] Choi G, Kim H S, Lee K, et al. Study on thermal conductivity and electrical resistivity of Al-Cu alloys obtained by Boltzmann transport equation and first-principles simulation: Semi-empirical approach. Journal of Alloys and Compounds, 2017, 727(15): 1237–1242.

[25] Billur C A, Gerçekcioglu E, Bozoklu M, et al. The electrical, thermal conductivity, microstructure and mechanical properties of Al-Sn-Pb ternary alloys. Solid State Sciences, 2015, 46: 107–115.

[26] Guo Y, Wang Y, Chen H T, et al. Anisotropic elasticity, electronic structure and thermodynamic properties of Al-Fe-Si intermetallic compounds from first principles calculations. Solid State Communications, 2019, 298: 113643.

[27] Wolverton C, Ozolins V. First-principles aluminum database: Energetics of binary Al alloys and compounds. Physical Review B, 2006, 73: 144104.

[28] Wang A J, Zhou L C, Kong Y, et al. First-principles study of binary special quasirandom structures for the Al-Cu, Al-Si, Cu-Si, and Mg-Si systems. CALPHAD: Computer Coupling of Phase Diagrams and Thermochemistry, 2009, 33(4): 769–773.

[29] Cui S, Jung I H. Thermodynamic modeling of the quaternary Al-Cu-Mg-Si system. CALPHAD: Computer Coupling of Phase Diagrams and Thermochemistry, 2017, 57: 1–27.
[30] Su C Y, Li D J, Luo A A, et al. Effect of solute atoms and second phases on the thermal conductivity of Mg-RE alloys: A quantitative study. Journal of Alloys and Compounds, 2018, 747: 431–437.
[31] Segall M D, Lindan P J D, Probert M J, et al. First-principles simulation: ideas, illustrations and the CASTEP code. Journal of Physics: Condensed Matter, 2002, 14: 2717.
[32] Perdew J P. Density-functional approximation for the correlation energy of the inhomogeneous electron gas. Physical Review B, 1986, 33: 8822–8825.
[33] Perdew J P, Burke K, Ernzerhof M. Generalized gradient approximation made simple. Physical Review Letters, 1996, 77: 3865–3872.
[34] Pfrommer B G, Côté M, Louie S G, et al. Relaxation of crystals with the Quasi-Newton method. Journal of Computational Physics, 1997, 131(1): 233–240.
[35] Mouhat F, Coudert F X. Necessary and sufficient elastic stability conditions in various crystal systems. Physical Review B, 2014, 90(22): 224104.
[36] Born M, Huang K. Dynamical theory of crystal lattices. Canada: Oxford University Press, 1954: 140–154.
[37] Watt J P. Hashin-shtrikman bounds on the effective elastic moduli of polycrystals with monoclinic symmetry. Journal of Applied Physics. 1980, 51: 1520–1524.
[38] Yildirim A, Koc H, Deligoz E. First-principles study of the structural, elastic, electronic, optical, and vibrational properties of intermetallic Pd_2Ga. Chinese Physics B, 2012, 21(3): 037101.
[39] Li S N, Ju X, Wan C B. Theoretical studies of elastic properties of orthorhombic $LiBH_4$. Computational Materials Science,2014, 81: 378–385.
[40] Long J P, Yang L J, Wei X S. First-principles study on the elastic property of hexagonal alunite. Physica B: Condensed Matter, 2012, 407(13): 2606–2609.
[41] Choi D H, Ahn B W, Queshel D J, et al. Behavior of β phase (Al_3Mg_2) in AA5083 during friction stir welding. Intermetallics, 2013, 35: 120–127.
[42] Cheng K M, Xu H X, Ma B C, et al. An in-situ study on the diffusion growth of intermetallic compounds in the Al-Mg diffusion couple. Journal of Alloys and Compounds, 2019, 810: 151878.
[43] Yao D M, Xia Y M, Qiu F, et al. Effects of La addition on the elevated temperature properties of the casting Al-Cu alloy. Materials Science and Engineering A, 2011, 528(3): 1463–1466.
[44] Andilab B, Ravineran C, Dogan N, et al. In-situ analysis of incipient melting of Al_2Cu in a novel high strength Al-Cu casting alloy using laser scanning confocal microscopy. Materials Characterization, 2020, 159: 110064.
[45] Hill R. The elastic behaviour of a crystalline aggregate. Proceedings of the Physical Society: Section A, 1952, 65(5): 349–354.
[46] Chen X Q, Niu H, Li D, et al. Modeling hardness of polycrystalline materials and bulk metallic glasses. Intermetallics, 2011, 19(9): 1275–1281.
[47] Mayer B, Anton H, Bott E, et al. Ab-initio calculation of the elastic constants and thermal expansion coefficients of Laves phases. Intermetallics, 2003, 11(1): 23–32.
[48] Pugh S F. XCII. Relations between the elastic moduli and the plastic properties of polycrystalline pure metals. The London, Edinburgh, and Dublin Philosophical Magazine and Journal of Science, 1954, 45(367): 823–843.
[49] Ravindran P, Fast L, Korzhavyi P A, et al. Density functional theory for calculation of elastic properties of orthorhombic crystals: applications to $TiSi_2$. Journal of Applied Physics, 1998, 84: 4891.
[50] Orson L A. A simplified method for calculating the debye temperature from elastic constants. Journal of Physics and Chemistry of Solids, 1963, 24(7): 909–917.
[51] Clarke D R. Materials selection guidelines for low thermal conductivity thermal barrier coatings. Surface and Coatings Technology, 2003, 163–164: 67–74.
[52] Cahill D G, Pohl R O. Lattice vibrations and heat transport in crystals and glasses. Annual Review of Physical Chemistry, 1988, 39: 93–121.
[53] Poirier P J. Introduction to the physics of the earth's interior. University of California Press, 2000.
[54] Shin J S, Ko S H, Kim K T. Development and characterization of low-silicon cast aluminum alloys for thermal dissipation. Journal of Alloys and Compounds, 2015, 644: 673–686.
[55] Chen D X. Analysis and research of hypoeutectic Al-Si alloy and eutectic Al-Si alloy in high thermal conductivity aluminum alloy design. Resource Recycling, 2019(1): 55–57.
[56] Wu Y N, Zhang J F, Liao H C, et al. Effect of homogenization temperature on microstructure and conductivity of Al-Mg-Si-Ce alloy. Journal of Materials Engineering and Performance, 2016, 25: 2720–2726.
[57] Zhang C, Du Y, Liu S H, et al. Microstructure and thermal conductivity of the as-cast and annealed Al-Cu-Mg-Si alloys in the temperature range from 25°C to 400°C. International Journal of Thermophysics, 2015, 36: 2869–2880.